SIGNATURE PAGE

This thesis for honors recognition has been approved for the

Department of Math & Engineering.

Willis D Weight — 12/6/18

Director — Date

Willis D. Weight

Print Name

Eric Sullivan — 12/4/2018

Reader — Date

Print Name

Gary Fischer — 12/6/2018

Reader — Date

Print Name

A Numerical Model of the Subaerial Landslide Generated Waves of the Berkeley Pit

Senior Thesis

Matthew McHugh

December 1, 2018

Abstract

Southwestern Montana has a very rich history because of its mining activities. Butte, home to the richest hill on earth, is no exception. Underground operations resulted in 10,000 miles of horizontal underground workings [1]. In 1950s the mining methods converted from underground to surface open-pit mining with the opening of the Berkeley Pit. In 1982 the pumps shut down and the Pit began receiving groundwater discharge. Slope instabilities along the Pit′s slopes result in occasional soil sloughs; in some instances, the sloughing generates a large enough volume of soil to propagate a wave across the Pit Lake. This is known as a landslide generated wave. This paper presents a numerical model that approximates the wave velocity and wave height of a landslide generated wave. The coupled model uses a simplified Navier-Stokes equation for wave velocity and the advection equation for wave height. The model successfully provides working boundary conditions; however, the instabilities of the numerical model inhibit verification of the model.

Contents

List of Figures

List of Tables

1 Introduction

Formerly an open pit copper mine, the Berkeley Pit is the collection of toxic water contaminated with dissolved heavy metals from groundwater discharge, precipitation, runoff, and snowfall. It is located in Butte, Montana, in Silver Bow County. The Berkeley Pit is projected to reach its critical water level of 5410 feet above sea level by July 2023 [7]. At this level, groundwater flow could overflow subsurface bedrock strata and become directed away from the Pit and therefore allow the toxic water to contaminate the local groundwater table. This scenario becomes more complicated by landslide generated waves created by sloughs on the Pit's unstable side-slopes. It arguably presents challenges in transporting the Pit's water to a water treatment plant.

A landslide generated wave is a wave that occurs when a submarine or subaerial landslide induces an impulsive force into a body of water [2]. Further, a landslide is considered submarine if the initial slide occurs beneath the water's surface, while a subaerial landslide begins its movement above the water's surface. The instability of the Berkeley Pit's sidewalls promotes the risk of a rotational failure resulting in a landslide [9]. In turn, a potential landslide creates the threat of a subaerial landslide generated wave, which produces a hazard for the hydraulic systems that transport the contaminated water from the Berkeley Pit to a water treatment plant. For instance, these waves would cause havoc in the operation and maintenance of a pump-barge system, which floats on top of the body of water and uses a suction pump to pull the water up through its pipes to a water treatment plant.

February 8, 2013 marks the latest sizeable slough, occurring on the southeast sidewall slopes [6]. The landslide measured 550 feet wide and generated 820,000 tons of material, which resulted in the water surface to rise 0.6 feet [6]. Over the past several years, the water level has been rising at a rate of approximately 0.65 feet per month [6]. The consistent rise in water level contributes to the instability of the walls, resulting in a higher chance slope failure.

As of June 4, 2018, the water level in the Berkeley Pit has exceeded an elevation of 5,347.24 feet above sea level [3]. The water level rises continually due to groundwater discharge, precipitation, snowfall, runoff, and the slumps of material from the sidewall slopes. The inevitability of reaching the critical water level means the impending decision of how and where to treat the water, and the selection of water treatment method must account for the possibility of aforementioned landslide-induced tsunami waves.

Various approaches have been developed to model tsunami waves caused by landslides. Researchers have developed numerical approximations and empirical equations to determine wave propagation. The uniqueness of this problem calls for a model with some simplifications, assumptions, and a few original, physics-based ideas. This paper presents a partial differential equation (PDE) model that can be used to numerically approximate the propagation of sub-aerial landslide generated waves by coupling wave velocity and wave height PDE's governed by a simplified Navier-Stokes equation and the advection equation, respectively.

2 The Berkeley Pit

2.1 History

Production from mining operations in the Berkeley Pit resulted in the extraction of approximately 320 million tons of ore and over 700 million tons of waste rock were mined from the Berkeley Pit [4]. By the end of the 19th century, Butte, Montana earned the nickname The Richest Hill on Earth due to the discovery and mining of gold, silver, and copper. Butte developed into a boomtown by World War I as a result of electricity′s high demand for copper. Copper became the trademark resource in the region. The year 1955 marked the highest copper prices since the end of World War I in 1918; however, open pit mining decreased jobs for local miners, and neighborhoods such as Meaderville, Dublin Gulch, and McQueen were forfeited with the expansion of open pit mining [4]. In 1955, excavation of what is now the Berkeley Pit–as well as open pit mining–began [4]. In 1982, a new owner of the mines, the Atlantic-Richfield Company (ARCO), suspended mining operations [4]. In the underground Kelley mine, 3900 feet deep, the operation of dewatering the underground mines and the Berkeley Pit ended on April 23, 1982 [4]. Even though underground mining had ceased seven years prior, the pumps in the underground mines continued to run in order to dewater the underground mines and the Berkeley Pit [4]. Shortly after the pumps were shut down, contaminated groundwater from the surrounding basin began seeping into the Pit [4]. The Berkeley Pit's lake filled due to flow from both groundwater and surface runoff; Berkeley Pit water is highly acidic, consisting of high concentrations of dissolved heavy metals.

ARCO shut down mining in the Continental Pit in 1983 [4]. Shortly after the suspension of mining, the United States Environmental Protection Agency (EPA) named the Berkeley Pit a federal Superfund site. The EPA defines a Superfund site as "an uncontrolled or abandoned place where hazardous waste is located, possibly affecting local ecosystems or people" (page 3) [4]. In 1985, ARCO sold some of its holdings to Dennis Washington; Washington restarted mining operations by his company, Montana Resources [4]. Today, the Butte Hill, with the Berkeley Pit at the epicenter, is one of the nation's largest federal Superfund site due to the high concentrations of copper, zinc, and other metals in the Pit Water.

2.2 General Information

Named after a historic underground mine, the Berkeley Pit measures approximately a mile in length, half a mile wide, and 1780 feet in depth [15]. The water in the Pit has a pH of about 2.5 and is contaminated with high concentrations of iron, copper, and other metals and metal salts [12]. Tests have been conducted on the Pit's water and sediment; in 2013, sloughing in the pit's walls dumped approximately 820,000 tons of soil into the pit, causing a massive 30-foot wave [6] [12]. This landslide generated wave displaced a sampling boat from the water surface and up onto a sidewall above the water surface. This event caused water monitoring to cease [12].

3 Landslide Generated Waves

3.1 General Information

The Department of Civil Engineering at Sharif University describes Landslide Generated Waves (LGW) as gravity-driven waves that occur when a submarine or subaerial landslide induces an impulsive force into a rigid body [2]. Landslides include naturally occurring gravity mass movements of soil, rock, lava, ice, and snow. A landslide is considered submarine if the initial slide occurs beneath the water's surface, while a subaerial LGW (SALGW) begins its movement above the water's surface. LGW's present a dangerous hazard to communities and infrastructure. Examples of LGWs that have caused destruction to communities as well as fatalities include the Alaska-Lituya Bay incident, Vajont Dam Reservoir in Italy, and the 1792 Unzen-Mayuyana incident in Norway [2]. The Alaska-Lituya Bay LGW occurred on July 9, 1958, when an earthquake generated at the Fairweather Fault shook loose approximately 40 million cubic yards of rock [14]. The rock fell from an elevation 3000 feet higher into the Northeast part of Lituya Bay [14]. This caused a wave that reached as high as 1720 feet, the largest recorded, and uprooted millions of trees on its way to spilling into the Gulf of Alaska, and propagated the entire length of Lituya Bay [14].

Instability in the walls of the Berkeley Pit causes the soil to slough off, which puts the Berkeley Pit at risk of landslide generated waves. Although the potential landslide mass is of significantly less magnitude than the 1958 Lituya Bay landslide, the Berkeley Pit landslides are large enough to induce a SALGW across the Pit. Unfortunately, Berkeley Pit LGW's have not been recorded or witnessed by Montana Resources (MR) nor British Petroleum (BP).

3.2 Berkeley Pit Slope Instability and Sloughs

Rotational sloughs caused by slope instabilities in soil are common in open pit mines. The greatest factor in the increasing slope instabilities of the Berkeley Pit sidewalls is the rising of Pit waters. Rain, snowfall, and occasional material sloughs from the pit's sidewalls affect the water levels. The most recent soil slump occurred in February of 2013, where an estimated 820,000 tons of material sloughed into the Berkeley Pit from the Southeast Wall [6]. It measured about 550 feet wide, and it caused the water level to rise approximately 0.6 feet [6]. Smaller landslides in August and November 2012 mark other recent sloughing events [5]. The November 2012 slough damaged the water quality sampling pontoon boat owned by Montana Resources, lifting it up onto the Pit's sidewall [5]. The 2013 event caused Montana Resources to restrain Montana Bureau of Mines and Geology (MBMG) scientists from sampling for safety reasons [5].

4 STRATA's 2015 Geotechnical Report

The paraphrased information throughout Section 4 and its subsections is from a geotechnical report performed by STRATA [9]. The side slopes of the Berkeley Pit are split into nine "sectors": the Northwest Wall, Southwest Wall, Neversweat, Colusa, Leonard, Concentrator, Southeast Corner, Pittsmont, and Northeast Corner.

STRATA, a professional services organization in geotechnical engineering and environmental consulting, completed a geotechnical report on October 22, 2015 on the side slopes of the Berkeley Pit. The report inspected the slope stability around the Berkeley Pit by reviewing past and current conditions, sampling and testing in the Pittsmont Sector, and drilling in the Concentrator Sector. STRATA's report also confirmed the critical water level to be 5410 feet at the Pilot Butte Mine. The primary, expected mode of failure for the Pit's walls are rotational failures. In certain sectors, minor sloughing could be caused by "thin, peel-like slope failures" (page 14) [9]. Slope stability depends on factors such as slope geometry, soil properties, and groundwater. STRATA's report states that "only those sectors containing fill material or native insitu alluvium at elevations in the pit walls that coincide with the pit water elevations are the areas most likely to be affected by slope instability as pit water level rises" (page 12) [9]. This means that the most unstable slopes are most likely where alluvium soil or fill encounters the water's surface. The greatest impact on increasing slope instability is the rising pit-water level in the Southeast Corner, Pittsmont, and Northeast Corner Sectors. The Concentrator Sector also could experience instabilities due to rising pit-water levels. These sectors contain mass amounts of insitu alluvium soil and overlying fill. According to STRATA, rising water levels will affect future slope instability the most in the south and east parts of the Berkeley Pit. The report provides the potential slope failure volumes for each sector, which is included in Section 4.

4.1 Sectors

Table 1 presents a table from STRATA's 2015 Geotechnical Report. The table proposed potential landslide material volumes caused by slope failures in the Berkeley Pit's sidewalls. The greatest potential slope failure volume would occur in the Concentrator sector at 668,400 cubic yards of soil. The following subsections discuss the likelihood of slope failure in each sector.

4.1.1 The Northwest Wall, Colusa, and Leonard Sectors

Typically, the most unstable slopes sport native in-situ alluvium soil or fill material. Adversely, the Northwest Wall, Colusa, and Leonard Sectors do not present a considerable threat of slope failure even though the three sectors store over 30 million cubic yards of fill . The fill is not likely to slide because it sits on bedrock at a minimum elevation of 5,543 feet. This elevation exceeds the CWL by over 100 feet; thus, the surface water will not reach the fill due to mandatory pumping and treatment once the water level reaches the CWL. Due to the difference in elevation, STRATA does not provide a potential slope failure volume because of the low risk of slope failure in these sectors [9].

4.1.2 The Southwest Wall

The soil material located in the Southwest Wall sector consists mostly of rock with minor amounts of fill and insitu alluvium. STRATA also does not provide a potential slope failure volume for this sector due to the unlikelihood of a sloughing event.

Table 1. Summary of General Slope Stability Conditions, Berkeley Pit

General Geologic Conditions	Sector	Approx. Elevation at Base of Fill (ft)	Approx. Elev. at Base of Alluvium (ft)	Potential Slope Failure Volume[1] (cu.yd.)
Primarily rock with minor amounts of fill or *insitu* alluvium	Northwest Wall	5,900	N.A.	None
	Southwest Wall	5,570 (Sec 32800) 5,450 (Sec 33800)	N.A.	None
Primarily rock with significant amounts of fill located above pit water level	Neversweat	5,480	N.A.	312,400[2]
	Colusa	5,705	N.A.	None
	Leonard	5,600	N.A.	None
Rock overlain by *insitu* alluvium and/or fill	Concentrator	5,450	5,430	668,400[3]
	Southeast Corner	5,400	5,240	208,300
	Pittsmont	5,380	5,200	511,100
	Northeast Corner	5,320	5,280	163,700
			Estimated Total Volume	*1,863,900*

[1]Estimate is based on assumption of shallow to mid-depth rotational slumps (per currently observed recent failure masses in the Southeast Corner, Pittsmont, and Neversweat Sectors).
[2]Slope failure due to continued erosion and undercutting by surface runoff, not due to rising pit water level.
[3]Includes potential failure volumes associated with the Bird Watch Dump.
Note: All elevations are referenced to the Anaconda datum, consistent with available cross-sections.

Table 1: STRATA proposed potential slough volumes by sector.

4.1.3 The Neversweat Sector

As in the case of the Northwest Wall, Colusa, and Leonard Sectors, the surface water will not reach the fill deposit in the Neversweat Sector. On the other hand, stormwater runoff presents the issue of erosion. Erosion causes undercutting of the fill slope. This type of instability would most likely result in minor and possibly thin, peel-like slope failures. STRATA believes that "large, deep-seated global slope failures are unlikely in this area" (page 14) [9]. The potential slope failure volume for the Neversweat Sector is 312,400 cubic yards. This estimated volume is based off a slope failure that is caused by erosion and undercutting of fill from surface runoff rather than rising pit water level.

4.1.4 The Concentrator Sector

The Concentrator Sector experiences erosion along the shoreline of the Bird Watch Dump (a part of this sector) due to wind-generated waves. This causes oversteepening and the possibility of minor sloughing; however, dump erosion from the waves does not impose major slope instabilities and therefore does not pose a high risk of slope failure. Mitigation measures to stabilize the Bird Watch Dump against wave action cannot be implemented. The eastern part of the Concentrator Sector is susceptible to steep, thin rotational slumps "breaking out through alluvium overlying the leached cap" (page 14) [9].

4.1.5 The Southeast Corner Sector

The alluvial soil in the Southeast Corner Sector is approximately 150 feet thick. Due to rising pit water levels, the saturation of the alluvium soil will likely increase. The increase in saturation will decrease the cohesion in the alluvium, which raises the chances of slope failure. Slope failure would again likely be a rotational, "peel-like" failure, similar to the failure in 2012.

4.1.6 The Pittsmont and Northeast Corner Sectors

The Pittsmont Dump, located in the Pittsmont and Northeast Corner Sectors, has the thickest compilation of insitu alluvium and overlying fill; therefore, this is the area of the Berkeley Pit where rising pit waters are most likely the have the greatest influence.

5 The Mathematical Model

5.1 Wave Velocity

5.1.1 Navier-Stokes Equations

The Navier-Stokes equations, derived from Newton's second law, are used to govern the motion of a real fluid. The equations consist of rates of change of fluid velocity in space and time, internal viscous forces, pressure gradient, and external forces such as gravity or electromagnetic fields. For this model, an incompressible condition is applied due to the relatively constant density of the pit water and also because we do not expect

significantly high pressures. Because the density is constant, the rate of change of density is zero and this term drops out of the Navier-Stokes equations. Given the incompressible condition $\nabla \cdot \vec{u} = 0$, the Navier-Stokes Equation takes the following form [13]:

$$\frac{\partial \vec{u}}{\partial t} + \vec{u} \cdot \nabla \vec{u} + \frac{\nabla P}{\rho} - \nu \nabla^2 \vec{u} = 0 \tag{1}$$

where $\vec{u}$ is the fluid velocity, P is the pressure, ρ is the fluid density, and ν is the kinematic viscosity of the fluid. In a wave, the pressure gradient represents the change in pressure caused by the accumulation, or "piling up", of water. The methods presented in this paper use a one-dimensional approach; therefore, equation (1) can be rewritten for $\vec{u}(\vec{x}, t)$, as shown in equation (2).

$$\frac{\partial \vec{u}}{\partial t} + \vec{u}\frac{\partial \vec{u}}{\partial x} + \frac{1}{\rho}\frac{\partial P}{\partial x} - \nu \frac{\partial^2 \vec{u}}{\partial x^2} = 0 \tag{2}$$

The external force gravity can be ignored in this instance because we are working in one-dimension, and there is no gravitational force in the x-direction.

5.1.2 Pressure Gradient and other terms

The pressure gradient represents the change in pressure between spatial points for all points in time. It is expressed as the pressure head created by the "piling up" of water by the wave. This pressure gradient supplements the velocity in the x-direction. Pressure head is calculated using the equation $P = \rho g y$, where ρ is the density of the water, g is gravitational acceleration, and y is the height of the wave; therefore, because of this pressure term, we can couple the wave velocity PDE with a PDE governing the height of the wave. If $H(\vec{x}, t)$ is wave height, then the pressure gradient can be approximated as $\nabla P = \rho g \frac{\partial H}{\partial x}$. The density term, ρ, drops out because the pressure gradient is divided by density as shown in the simplified Navier-Stokes equation (2).

5.2 Wave Height

Since the pressure gradient relates to the change in the height of the wave, the wave velocity equation can be coupled with an equation for wave height. In one-dimension, the wave height equation will determine the propagation of the wave, which is a necessary demonstration for the purpose of this research, regardless if we need it to determine the wave velocity or not. The partial differential equation used to determine the wave height propagation is the advection equation with an added, minor viscosity term for smoothing purposes. The advection equation plus the viscous smoothing term resembles the non-linear, viscous Burgers' equation (the smoothing term is non-physical and is included to increase stability of the numerical methods explored in Section 6; therefore, we take the coefficient ν_2 to be very small). The final form of the wave height equation is:

$$\frac{\partial H}{\partial t} + \vec{u}\frac{\partial H}{\partial x} - \nu_2 \frac{\partial^2 \vec{u}}{\partial x^2} = 0 \tag{3}$$

where $H(\vec{x}, t)$ is the wave height and ν_2 is the non-physical, very small viscosity term. The following list summarizes the assumptions taken in this mathematical model:

1. The landslide starts at the soil-water interface rather than at an elevation above the Pit lake.
2. The volume of soil submerged in the Pit lake from the landslide with respect to time is governed by a linear function.
3. The velocity of the slide is uniform.
4. We assume perfect energy conversion at the boundary (no friction loss)–the boundary conditions will be explained in Section 6.

6 Numerical Methods

Due to the inability to solve non-linear partial differential equations, such as the Navier-Stokes equations, numerical methods must be used in order to approximate a solution. The computer software used for the research presented in this paper was MatLab [8]. This paper uses finite difference methods to approximate the wave velocity and height. The methods used produce instabilities that do not allow the velocity or height plots to propagate for the entirety of the landslide; thus, future work would include exploring other approximation methods that increase the stability of the model. Such methods are described in Section 7 at the conclusion of this paper.

6.1 Discretization

We used a Finite Difference Model (FDM) numerical scheme, which stems from Taylor approximations, to approximate the derivatives in the model. Various time and spatial derivative approximations were considered. The schemes that were attempted include Euler, Leapfrog, and Lax-Wendroff approximations for the time derivative and an upwind scheme of varying orders for the spatial first derivative. The second derivative viscosity term is approximated using a first order, centered, second derivative approximation. Additionally, the numerical approximation of the model requires initial conditions for the variable in time and boundary conditions for the variable in space.

This paper explores two different discretization techniques for the first partial derivative in space: a 1st order upwind scheme and a 2nd order upwind scheme. The time derivative approximation uses an Euler step, the viscosity term uses a first order, second derivative, centered scheme, and the pressure term uses a first order first derivative approximation. Further definitions of the aforementioned numerical methods are included in Appendix A. The following systems of equations illustrate the model using different discretization methods:

$$\begin{cases} \frac{U_j^{n+1}-U_j^n)}{dt} = -U_j^n \frac{U_j^n - U_{j-1}^n}{dx} + \nu \frac{U_{j+1}^n - 2U_j^n + U_{j-1}^n}{dx^2} - g\frac{H_j^n - H_{j-1}^n}{dx} \\ \frac{H_j^{n+1}-H_j^n}{dt} = -U_j^n \frac{H_j^n - H_{j-1}^n}{dx} + \nu_2 \frac{H_{j+1}^n - 2H_j^n + H_{j-1}^n}{dx^2} \end{cases} \tag{4}$$

$$\begin{cases} \frac{U_j^{n+1}-U_j^n}{dt} = -U_j^n \frac{3U_{j+1}^n - 4U_j^n + U_{j-1}^n}{2dx} + \nu \frac{U_{j+1}^n - 2U_j^n + U_{j-1}^n}{dx^2} - g\frac{H_j^n - H_{j-1}^n}{dx} \\ \frac{H_j^{n+1}-H_j^n}{dt} = -U_j^n \frac{3H_{j+1}^n - 4H_j^n + H_{j-1}^n}{dx} + \nu_2 \frac{H_{j+1}^n - 2H_j^n + H_{j-1}^n}{dx^2}. \end{cases} \tag{5}$$

Equation (4) displays the system of equations' discretizations using finite difference schemes with the first order upwind spatial first derivative, while equation (5) exhibits the slight modification of using a second order spatial first derivative. The notation U_j^n is defined as $U(\vec{x_j}, t_n)$, where j is the spatial discretization step and n is the temporal discretization step. The same notation is used for the height function, H.

6.2 Boundary Conditions

The boundary condition in one dimension dictates the first spatial point for all points in time. There is no boundary condition for the last spatial point, the the pit wall opposite of where the landslide occurs, because the instabilities in the model does not allow the wave propagation to reach the edge boundary. The boundary is controlled by the interaction of the soil mass of the landslide and the pit lake at the first spatial point. A few assumptions are taken to further define the landslide-pit lake interaction: the landslide is taken to commence at the interface of the pit's wall and its lake and the landslide mass enters the lake only at the first spatial point. This model takes the simplification that the motion of the landslide volume can be described using a linear equation. The equation

$$V_{sub} = \frac{V_{tot}}{t^*} t \tag{6}$$

dictates the volume of soil submerged. The variable V_{sub} is the submerged soil volume, V_{tot} is the total volume of the slide, and t^* is the total time that the landslide is in motion. The V_{tot} value is extracted from the STRATA geotechnical report, which estimates landslide volumes caused by potential slope failures.

The following boundary conditions for wave velocity and wave height exist for the time of the landslide, t^*. After the time of the slide, there is no more soil volume driving a change in velocity or height at the boundary; thus, we can take the first spatial point to be zero for all time after the landslide. Likewise, we take the wave height and velocity to be zero for all times before the landslide commences; this reasoning drives the initial conditions that will be discussed in Section 6.3. Both the boundary and initial conditions exist under the assumption that the wave starts when the landslide starts.

6.2.1 Wave Velocity

Discretization 1 The system of equations given by equation (4) presents finite difference methods including an Euler time step scheme, a first order upwind spatial first derivative scheme, and first order centered second derivative scheme. Since the finite difference methods used are all first order, the model requires one piece of information. This piece of information is the boundary condition; thus, we need a physical relation between the landslide and the pit water that controls the wave height at the first spatial step. From (cite the research), the velocity of the slide mass can be described by Newtownian physics (when not treated as a granular mass), as displayed by equation 7:

$$v_{slide} = f_s g t cos(\theta) \tag{7}$$

where v_{slide} is the velocity of the landslide, g is gravitational acceleration, t is time, and θ is the angle of the pit wall with the horizontal. The variable f_s is the fraction of landslide volume that is unsubmerged and is related to the linear submerged volume equation by the expression $\frac{V_{slide}-V_{sub}}{V_{slide}}$. The boundary condition for the wave velocity is the velocity at the boundary. We can use energy conservation at the boundary, which is where the landslide enters the pit lake and the first spatial point of the model, to determine the boundary condition. Under the assumption of perfect energy conversion and no frictional loss, meaning that the landslide is essentially a free falling body, we can equate the kinetic energy of the landslide at the boundary to the kinetic energy and the potential energy of the wave at the boundary. We can extract the wave velocity from the equation for kinetic energy of the wave to attain the boundary condition. The following equations express the conservation of energy at the boundary:

$$KE_{slide} = KE_{wave} + PE_{wave} \tag{8}$$

$$\frac{1}{2} m_{slide} v_s^2 = \frac{1}{2} m_{wave} v_w^2 + m_{wave} g H. \tag{9}$$

The energy conversion occurs at each point in time; thus, we need to determine the amount of energy provided by the landslide at each point in time. The mass of the landslide, m_{slide}, can be calculated by multiplying its density by its volume–the volume at each point in time can be determined by taking the difference of the volume submerged at the current point and the previous point. Since the volume of soil submerged equals the volume of water displaced, we calculate the mass of the wave at the boundary the same way, except using the density of the water rather than the soil. The height of the wave, H, comes from the wave height PDE at the first spatial point. The energy conversion equation therefore takes the form:

$$\frac{1}{2}(\rho_s(V_s^n - V_s^{n-1}))v_s^2 = \frac{1}{2}(\rho_w(V_s^n - V_s^{n-1}))v_w^2 + (\rho_w(V_s^n - V_s^{n-1}))gH_1^n. \tag{10}$$

We can solve for the velocity of the wave at the boundary for all points in time, U_1^n (v_w in 10). This results in our boundary condition:

$$v_w = U_1^n = \sqrt{\frac{(\rho_s(V_s^n - V_s^{n-1}))v_s^2 - 2(\rho_w(V_s^n - V_s^{n-1}))gH_1^n}{(\rho_w(V_s^n - V_s^{n-1}))}} \tag{11}$$

Discretization 2 The system of equations given by equation (5) presents finite difference methods including an Euler time step scheme, a second order upwind spatial first derivative scheme, and first order centered second derivative scheme. Since the second order upwind scheme for the spatial first derivative requires two pieces of information, we need two boundary conditions. From [cite the document], The first boundary condition uses Newtonian physics to calculate the landslide velocity [11]; it assumes perfect energy conversion from the slide mass to the water at the boundary. The boundary condition at the first spatial point remains the same and is represented by equation 11. The second boundary condition uses a first order upwind scheme for the first spatial derivative, just like in the first discretization, but only for the second spatial step. The second order upwind spatial first derivative method takes over at the third spatial point. Equation 12 represents the second boundary condition:

$$U_2^{n+1} = U_2^n + dt\left(-U_2^n\frac{U_2^n - U_1^n}{dx} + \nu\frac{U_3^2 - 2U_j^n + U_1^n}{dx^2} - g\frac{H_2^n - H_1^n}{dx}\right). \tag{12}$$

6.2.2 Wave Height

The first wave height boundary condition relates the submerged landslide mass to the wave height; this works under the assumption that the volume of the landslide submerged in the pit lake is equal to the displaced volume of water. This model assumes that soil from the landslide enters the water at the same time that the landslide starts.

Discretization 1 Given the aforementioned assumptions, we can state that the wave height at the boundary equals the amount of water displaced by the submerged soil volume; therefore, the integral of the wave profile at any point in time equals the amount of landslide that has been submerged at that same point in time. Using the assumption that the accumulated wave height equals the submerged landslide volume at each point in time,

$$\int H^n dx = \frac{V_s^n}{b},$$

we can approximate the integral using a Riemann sum and solve for the wave height at the boundary. This gives us the boundary condition at the first spatial point

$$H_1^n = \frac{V_s^n}{b\Delta x} - \sum_j H_j^n, \tag{13}$$

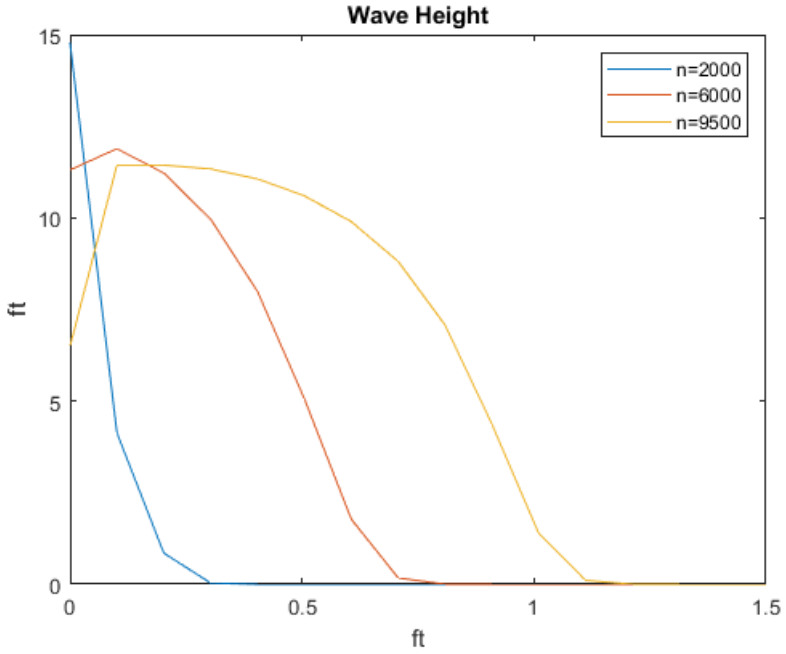

Figure 1: Wave height profiles at three different time steps.

where b is the width of the landslide and V_s is the submerged volume of the landslide as a function of time.

Discretization 2 As previously discussed, we need a second boundary condition for the second discretization. The first spatial point is determined by the boundary condition used for the first discretization, and the second spatial point is determined by a first order upwind scheme for the spatial first derivative. The second boundary condition is determined by

$$H_2^{n+1} = H_2^n + \Delta t \left(-U_2^n \frac{H_2^n - H_1^n}{dx} + \nu_2 \frac{H_3^n - 2H_2^n + H_1^n}{dx^2} \right), \tag{14}$$

where H_j^n is the height of the wave, U_j^n is the velocity of the wave, and Δt is the time step.

6.3 Initial Conditions

The initial conditions dictate the velocity and height of the wave before the landslide starts. The initial condition for the wave velocity is zero because the water is not moving until the landslide mass begins to submerge into the lake. The wave height initial condition is also zero because the wave does not grow until the landslide mass begins to submerge into the lake.

6.4 Images of the Model

6.4.1 Discretization 1

Figures 1, 2, 3, and 4 display snapshots in time of the model using the first discretization method discussed previously in Section 6. The black ellipses on Figures 2and 4 point out the instabilities in the model.

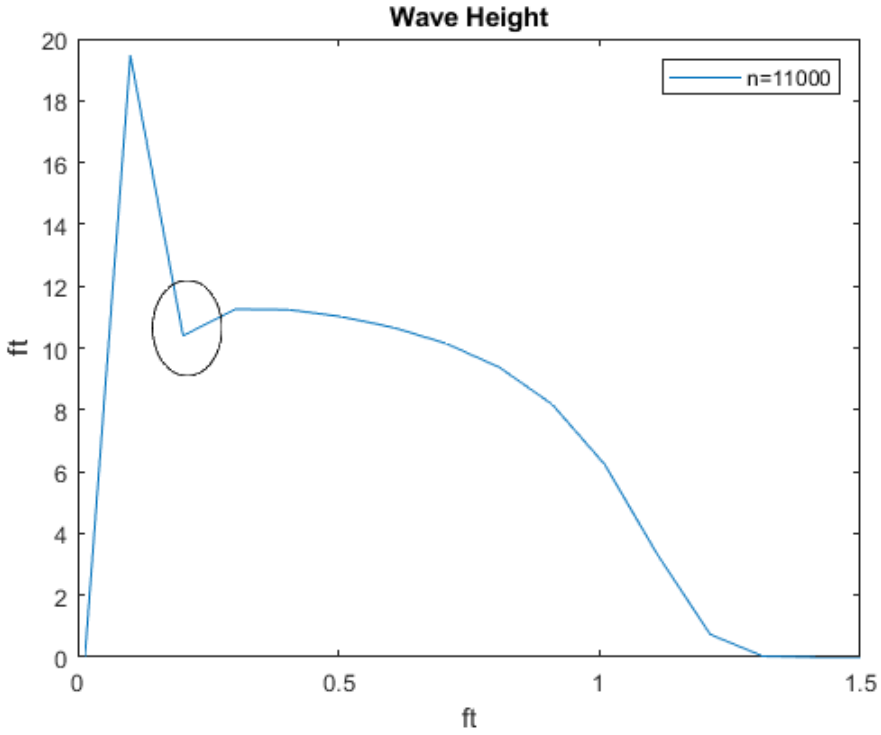

Figure 2: Wave height profile after the model becomes unstable.

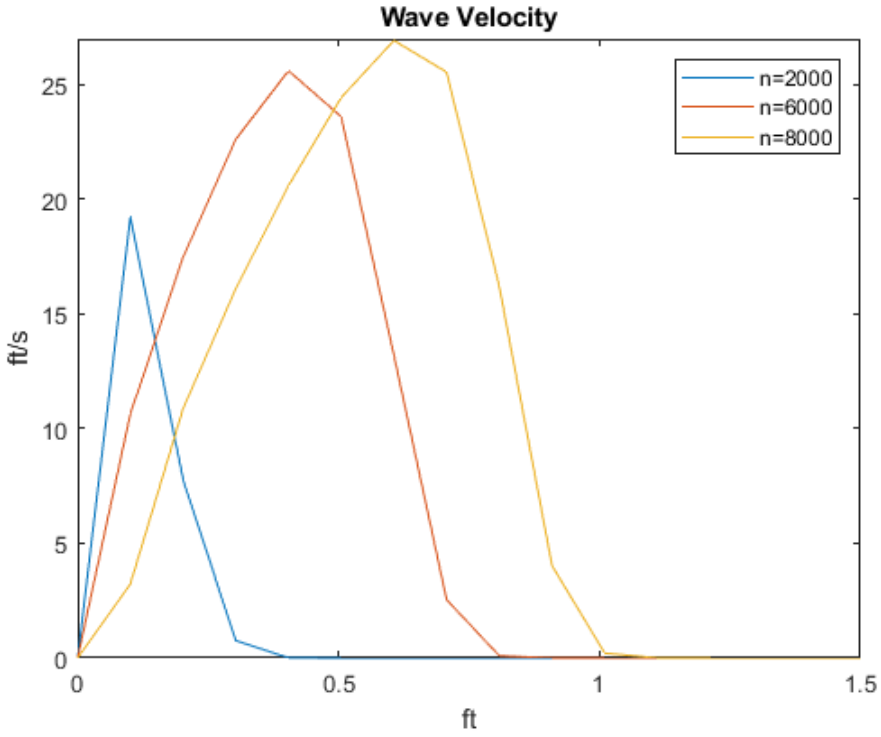

Figure 3: Wave velocity profiles at three three different time steps.

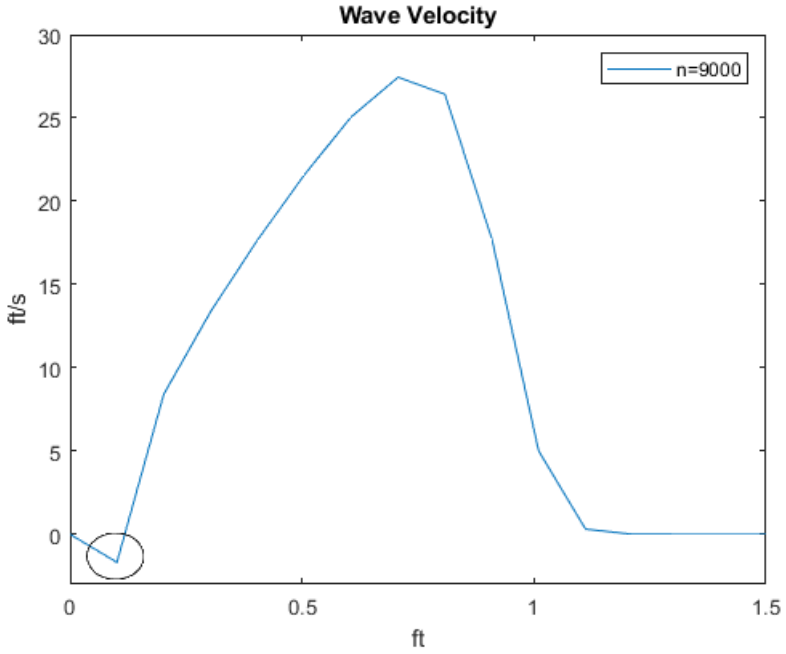

Figure 4: Wave velocity profile after the model becomes unstable.

6.4.2 Discretization 2

Figures 5, 6, 7, and 8 display snapshots in time of the model using the second discretization method discussed previously in Section 6. The black ellipses on Figures 6 and 8 point out the instabilities in the model.

6.5 Successes of the Model's Numerical Approximation

Although the instabilities of the model greatly impede the visual perception of the model, this model still provides numerous successes.

- Given the assumptions, this paper provided working boundary conditions that make sense physically
- The model couples the simplified Navier-Stokes equation for wave velocity with the advection equation for wave height; thus, we get both velocity and height simultaneously.
- We were able to simplify the motion of the landslide in order to avoid expressing it as a granular media, which would have extended the scope of work outside of the alotted time for this paper.
- We can recognize the complexities of the given problem; some are due to limited information and some because it is a challenging and complex problem.

6.6 Failures of the Model's Numerical Approximation

Failures of this model include:

- The numerical approximation exhibits instabilities, and those instabilities develop quickly. In fact, they develop before we can observe the wave after the landslide stops dumping soil mass into the pit lake.

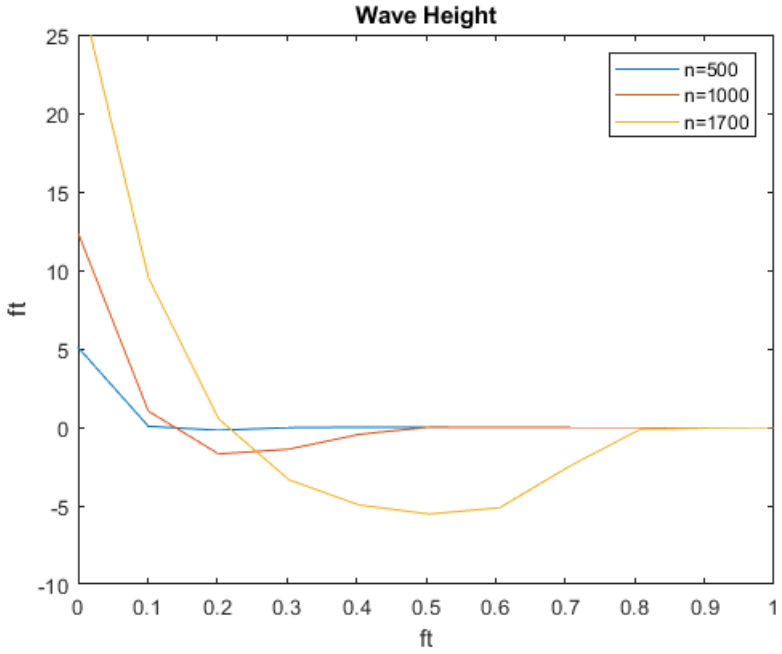

Figure 5: Second Discretization: Wave height profiles at three different time steps.

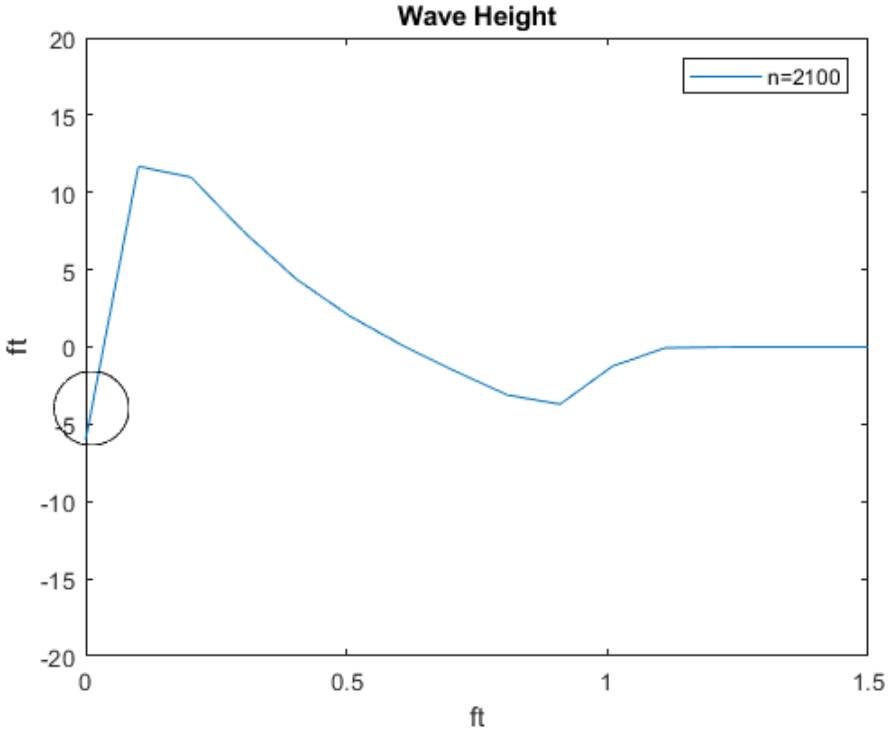

Figure 6: Second Discretization: Wave height profile after the model becomes unstable.

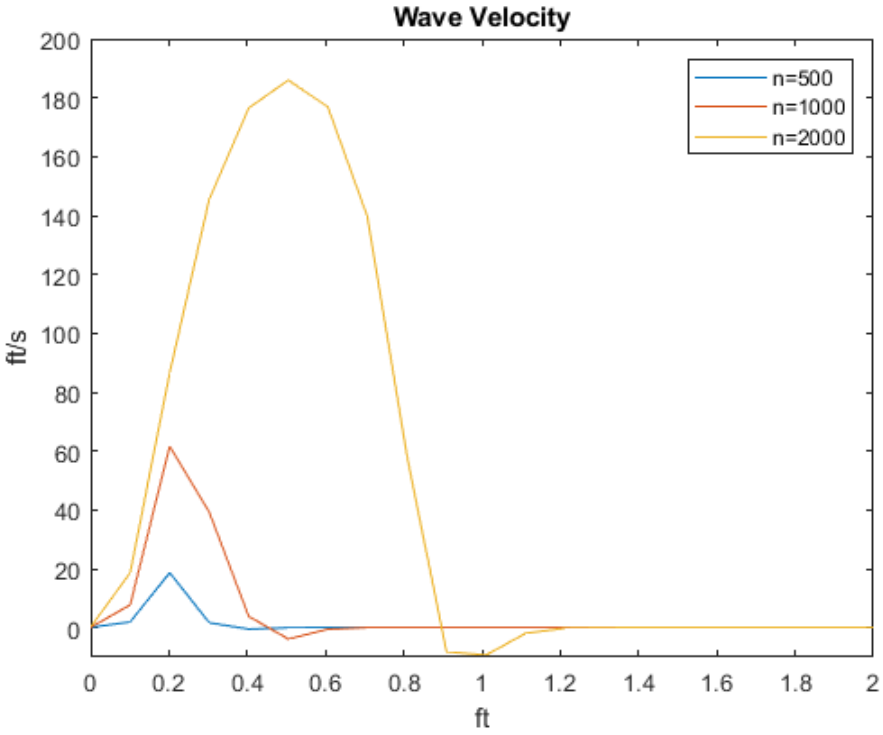

Figure 7: Second Discretization: Wave velocity profiles at three three different time steps.

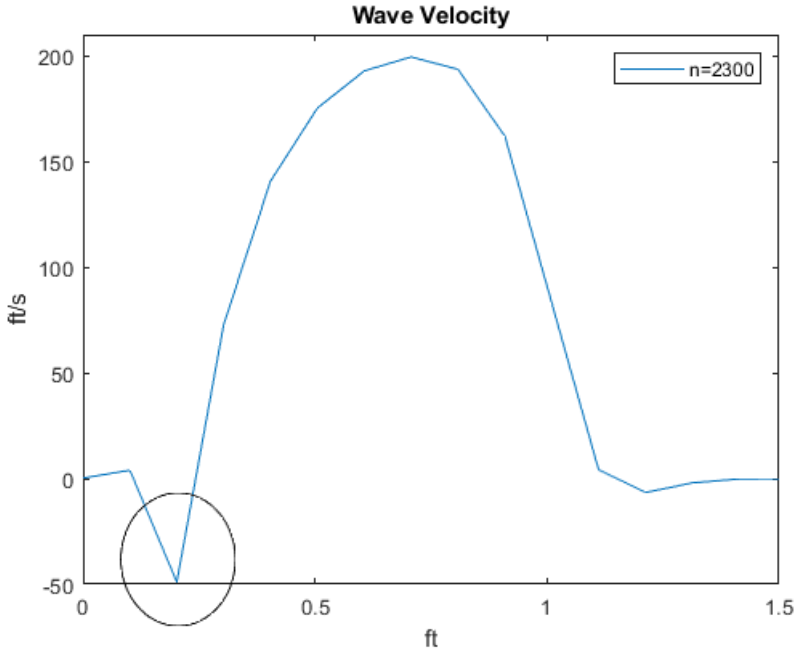

Figure 8: Second Discretization: Wave velocity profile after the model becomes unstable.

- Due to the issues with stability, we were not able to limit the number of assumptions/simplification made in our model, nor were we able to analyze or explore different parts of our model.
- There is no validity assessment for this model due to the lack of field measurements or information that could be compared to our results. Even if this information was available, we do not have many results to compare due to the instabily of the model.

7 Future Work

Future work to improve this model include:

- Explore using the KDV equation to govern wave height propagation rather than the advection equation.
- Use Finite Volume Methods rather than Finite Difference Methods for approximating spatial derivatives, or more robust Finite Difference Methods, to check for improvements in stability.
- Use McCormack's method for temporal derivatives to check for improvements in stability.
- Limit assumptions and/or simplifications such as coupling a granualar media landslide model to the wave equations and analysis of different types of functions governing the landslide motion
- observations, videos, and/or measurements of actual Berkeley Pit LGW's would allow a validity assessment for a stable model.

References

[1] "Butte Montana: A Case for the Mining Metropolis". [Online]. Available: https://scenariojournal.com/article/butte-montana/

[2] "Subaerial Landslide-Generated Waves: Numerical and Laboratory Simulations". [Online]. Available: https://link.springer.com/chapter/10.1007/978-3-319-59469-9_3. [Accessed: 6-Jan-2018].

[3] "Water Levels". [Online]. http://www.pitwatch.org/waterlevels/ [Accessed: 27-Nov-2018].

[4] "Berkeley Pit History". [Online]. Available: http://www.pitwatch.org/berkeley-pit-history/ [Accessed: 20-Nov-2017],

[5] "Study Details Slope Stability". [Online]. Available: http://www.pitwatch.org/study-details-slope-stability/ [Accessed: 20-Nov-2017].

[6] "Berkeley Pit Slough". [Online]. Available: http://www.pitwatch.org/berkeley-pit-slough/ [Accessed: 8-Jan-2018].

[7] "Water Level Rising More Slowly than Originally Projected". [Online]. Available: http://www.pitwatch.org/water-level-rising-more-slowly-than-originally-projected/ [Accessed: 6-Jan-2018].

[8] "MathWorks". [Online]. Available: https://www.mathworks.com/ [Accessed: 1-Nov-2017].

[9] "Final BMFOU Berkeley Pit Slope Stability Evaluation STRATA Report". [Online]. https://semspub.epa.gov/work/08/1549496.pdf [Accessed 1-Dec-2017].

[10] "An Introduction to the Incompressible Euler Equations". [Online]. Available: https://www.math.ucdavis.edu/~hunter/notes/euler.pdf [Accessed: 29-Sep-2017].

[11] "Numerical Modeling of Tsunami Generation by Subaerial and Submerged Landslides". [Online]. ftp://ftp.mohid.com/Fortaleza_CD/Bibliografia/Waves/Tsunamis/Tsunami%20numerical%20modeling.pdf [Accessed: 01-Oct-2017].

[12] "Life from the Pit". [Online]. Available: https://medium.com/vision-2018/life-from-the-pit-70d3e0fbc0f6. [Accessed: 8-Apr-2018].

[13] http://mathworld.wolfram.com/Navier-StokesEquations.html

[14] https://geology.com/records/biggest-tsunami.shtml

[15] "The Berkeley Pit". [Online]. Available: https://www.atlasobscura.com/places/berkeley-pit. [Accessed: 8-Jan-2018].

A Discretization

Method	Derivative	Discretization
Euler Step	$\frac{\partial U}{\partial t}$	$\frac{U_j^{n+1}-U_j^n}{dt}$
1st Order Upwind	$\frac{\partial U}{\partial x}$	$\frac{U_j^n-U_{j-1}^n}{dx}$
2nd Order Upwind	$\frac{\partial U}{\partial x}$	$\frac{3U_{j+1}^n-4U_j^n+U_{j-1}^n}{dx^2}$
1st Order Centered	$\frac{\partial^2 U}{\partial x^2}$	$\frac{U_{j+1}^n-2U_j^n+U_{j-1}^n}{dt}$

B Matlab Code

```
%Discretization 1

clear;clc;clf; close all;

tmin = 0;

tmax = 0.5;

numpts_t = 100000;

t = linspace(tmin,tmax,numpts_t);

xmin = 0;

xmax = 10;

numpts_x = 100;

x = linspace(xmin,xmax,numpts_x);

dt = t(2) - t(1);

dx = x(2) - x(1);

U = zeros(length(x),length(t));

H = zeros(length(x),length(t));

t_star = 0.1;

Vol_slide_cy = 1;

Vol_slide_cf = Vol_slide_cy * 27 ;

b = .05*27;

rho = 4.35;

g = 32.2;

theta = pi/4 ;

rho_w = 62.4 / g ;

Vs(1) = 0 ;

for n = 1:length(t)-1

        if (t(n) >= 0) && (t(n) < t_star)

        Vs(n+1) = (Vol_slide_cf/t_star)*t(n+1);

        U(1,1) = 0 ;

        U(1,n+1)=  (Vol_slide_cf-Vs(n+1))/Vol_slide_cf * g * t(n+1)* cos(theta);
```

```
        H(1,n+1) = Vs(n) / (b * dx) - sum(H(2:end,n)* dx )/dx ;
        U(2:end-1,n+1) = U(2:end-1,n) + dt * ( - ( ( U(1:end-2,n)+U(2:end-1,n))/2).*(U(2:end-1,n)
            -U(1:end-2,n))/dx+ (10^-6)/(dx^2)*(U(3:end,n)
            - 2*U(2:end-1,n) + U(1:end-2,n)) - (g/dx)
            * (H(2:end-1,n)-H(1:end-2,n)));
        H(2:end-1,n+1) = H(2:end-1,n) + dt
            * ( - ( ( U(1:end-2,n)+U(2:end-1,n))/2).*(H(2:end-1,n)
            -H(1:end-2,n))/dx ...
            + 0.00000001/(dx^2)*(H(3:end,n)
            - 2*H(2:end-1,n) + H(1:end-2,n)));
        else
        U(1,:) = 0;
        H(1,:) = 0;
            U(2:end-1,n+1) = U(2:end-1,n) + dt * ( - ( ( U(1:end-2,n)
                +U(2:end-1,n))/2).*(U(2:end-1,n)-U(1:end-2,n))/dx
                + 0.0001/(dx^2)*(U(3:end,n) - 2*U(2:end-1,n) + U(1:end-2,n))
                - (g/dx)* (H(2:end-1,n)-H(1:end-2,n)));
            H(2:end-1,n+1) = H(2:end-1,n) + dt * ( - ( ( U(1:end-2,n)
                +U(2:end-1,n))/2).*(H(2:end-1,n)-H(1:end-2,n))/dx ...
                + 0.000001/(dx^2)*(H(3:end,n) - 2*H(2:end-1,n) + H(1:end-2,n)));
        end
end

%Discretization 2
clear;clc;clf; close all;
tmin = 0;
tmax = 0.5;
numpts_t = 100000;
t = linspace(tmin,tmax,numpts_t);
xmin = 0;
xmax = 10;
numpts_x = 100;
x = linspace(xmin,xmax,numpts_x);
dt = t(2) - t(1);
dx = x(2) - x(1);
U = zeros(length(x),length(t));
H = zeros(length(x),length(t));
```

```
t_star = 0.1;
Vol_slide_cy = 1;
Vol_slide_cf = Vol_slide_cy * 27 ;
b = .05*27;
rho = 4.35;
g = 32.2;
theta = pi/4 ;
rho_w = 62.4 / g ;
Vs(1) = 0 ;
for n = 1:length(t)-1
        if (t(n) >= 0) && (t(n) < t_star)
        Vs(n+1) = (Vol_slide_cf/t_star)*t(n+1);
        U(1,1) = 0 ;
        H(1,1) = 0;
        U(1,n+1)=  (Vol_slide_cf-Vs(n+1))/Vol_slide_cf * g * t(n+1)* cos(theta);
        H(1,n+1) = Vs(n) / (b * dx) - sum(H(2:end,n)* dx )/dx ;
        U(2,n+1) = U(2,n)+ dt*(-U(2,n).*((U(2,n)-U(1,n))/(dx))+(10^-6)
            *((U(3,n)-2*U(2,n)+U(1,n))/(dx^2))...
            -(g/dx)*((H(2,n)-H(1,n))));
        H(2,n+1) = H(2,n) + dt * (-U(2,n).*((H(2,n)-H(1,n))/(dx))
            +0.00000001*((H(3,n)-2*H(2,n)+H(1,n))/(dx^2)));
        U(3:end,n+1) = U(3:end,n) + dt * (-(U(3:end,n)+U(2:end-1,n)
            + (10^-6)/(dx^2) * (U(3:end,n)-2*U(2:end-1,n)+U(1:end-2,n))/(dx^2)
            - (g/dx) * (H(3:end,n)-H(2:end-1,n))/dx);
        %non-linear term contains a calculation for average velocity for stability purposes
        H(3:end,n+1) = H(3:end,n) + dt * ( - U(3:end,n).*(3*H(3:end,n)
            -4*H(2:end-1,n)+H(1:end-2,n))/dx ...
            + 0.00000001/(dx^2)*(H(3:end,n) - 2*H(2:end-1,n) + H(1:end-2,n)));
        else
        U(1,:) = 0;
        H(1,:) = 0;
        U(3:end,n+1) = U(3:end,n) + dt * ( -U(3:end,n).*(3*U(3:end,n)
            -4*U(2:end-1,n)+U(1:end-2,n))/(2*dx) ...
            + (10^-6)/(dx^2) * (U(3:end,n)-2*U(2:end-1,n)+U(1:end-2,n))/(dx^2)
            - (g/dx) * (H(3:end,n)-H(2:end-1,n))/dx);
        H(3:end,n+1) = H(3:end,n) + dt * ( - U(3:end,n).*(3*H(3:end,n)
            -4*H(2:end-1,n)+H(1:end-2,n))/dx ...
```

```
            + 0.00000001/(dx^2)*(H(3:end,n) - 2*H(2:end-1,n) + H(1:end-2,n)));
        end
end
```